

High Level Trigger Using ALICE ITS Detector

A. K. Mohanty

CERN, CH-1211, Geneva 23, Switzerland

Abstract

The high P_T trigger capabilities of the ALICE inner tracking system (ITS) as a standalone detector have been investigated. Since the high P_T charged particles mostly lead to the linear trajectories within this ITS sector, it is possible to select tracks of P_T of the order of 2 GeV and above by confining to a narrow search window in the (θ, ϕ) space. Also shown that by performing a principal component transformation, it is possible to rotate from a 12 dimensional $(\theta-\phi)$ space (in this space, a good ITS track has 6 pairs of hit co-ordinates) into a parametric space characterized by only two independent components when the track momentum exceeds a particular limit. This independent component analysis (ICA) has been utilised further to reduce the false track contribution to an acceptable level particularly when the charged multiplicity is large. Finally, it is shown that with a narrow bin width of $\Delta\theta = \Delta\phi \sim 0.008$ radian and with PCA or ICA cut, the ITS can be used to trigger the jet particles with $P_T \geq 2$ GeV. Apart from triggering these high P_T particles, this method can also be used to estimate the initial momentum of the high P_T tracks for seeding which can be further prolonged into the TPC detector both for offline and online Kalman tracking or even to detect those high P_T tracks of rare events which might get lost in the TPC-TRD dead zone.

I. INTRODUCTION

ALICE (A Large ION Collider Experiment) has a dedicated detector systems to study the collective properties of the hot and dense matter created in nucleus-nucleus collisions using the CERN large hadron collider (LHC) in the year ~ 2007 . The ALICE detectors will measure and identify mid-rapidity hadrons, leptons and photons produced in the interactions [1]. The design parameters of the ALICE detectors are optimized to cope with multiplicities up to 8000 charged particles per unity rapidity (the theoretical prediction of $dN_{ch}/d\eta$ at mid-rapidity for PbPb collision at $\sqrt{s} = 5.5$ A TeV may lie between 2000 and 6000), resulting in 20000 charged primary and secondary tracks in the acceptance of the central detector systems that covers mid-rapidity $-0.9 \leq \eta \leq 0.9$ and full azimuth. Based on current physics simulations, the central event size in Pb-Pb interaction is expected to be about 86 MB before compression out of which about 75 MB of raw data is generated by the time projection chamber (TPC), which is the main tracking device of the ALICE detector (A brief description of the ALICE detector systems is given in the appendix and also can be found in ALICE PPR [1] and reference therein). Several data compression algorithms have been tried on simulated TPC data [2]. Using Huffman compression and an optimized frequency distributioni we have also shown that it is possible to achieve a lossless compression ratio of $\sim 50\%$ on the realistic TPC rawdata that includes read out overheads [3,4]. An estimate of the total bandwidth needed for the data transfer requires evaluation of the rawdata throughput for each type of trigger. The number of events required to accumulate enough statistics in one year period of data taking (which has an effective time of 10^6 s) is a few 10^6 events for hadronic physics, a few 10^7 events for minimum bias, hadronic charm and electron physics and at least 10^9 for dimuon physics. The needed rates are then of the order of a few Hz for hadronic physics, a few tens of Hz for minimum bias, hadronic charm and electrons and a few hundreds of Hz for dimuons for the L2 triggers. At a read out frequency of 200 Hz, a total band width of ~ 15 GB/s coming out of the detector has to be handled

(This rate roughly coincides with the TPC limitation ¹).

Thus, the amount of data which needs to be written to mass storage will be about a few PBytes per year. One of the major objective of the ALICE experiment is to measure rare processes such as jet transverse energy spectra up to $E_T \sim 200$ GeV and the pattern of medium induced modifications of charmonium and bottomium bound states. These low cross section rare events (which range down to one in 10^7 pp and to one in 10^4 PbPb events), require full exploitation of all the available luminosity in order to attain the desired event statistics and will generate data volume which will far exceed what can be transferred to the permanent storage system. ALICE would not be able to acquire sufficient statistics for many rare probes without rejecting many unwanted events by sharpening the momentum cut through a high level trigger (HLT) mechanism. Therefore, the HLT system is one of the important aspect of the ALICE detectors which controls the data flow between the front end electronics of the detectors and the event builder of the data acquisition system. Using simulated rawdata, all the present HLT studies examine the possibility of having a fast cluster finder (using techniques like Hough transformation etc) leading to a fast pattern recognition algorithm primarily for the tracks in the TPC sectors [5,6]. In this work, we consider the possibility of generating a high P_T trigger using the hit informations only from the ITS sectors of the ALICE detectors where all high P_T charged particle trajectories are mostly linear. As will be shown later, using a simple road-finder algorithm based on a narrow (θ, ϕ) search window, it has been possible to reject significant amount of low P_T backgrounds.

¹At an average luminosity of $10^{27} \text{ cm}^{-2} \text{ s}^{-1}$, the minimum bias rate (assuming 8 barn total cross section) for PbPb collision is 8 KHz out of which 1 KHz may be considered as central events. At this event rate, ($f = 8000$ events/s), and with drift time $\tau = 90 \mu\text{s}$, the fraction of PbPb double events in the TPC is $[1 - \exp(-2\tau_{drift} f)] = 0.76$, where 2τ accounts for the past and present memory of the TPC. The clean minimum bias PbPb events thus reduces to about 1900 Hz and the central rate to about 240 Hz.

It has been possible to extract the momentum of these tracklets through a χ^2 minimization procedure which agree well (within 20%) with the actual momentum. The computation is also fast enough as the track density is very low within a small $\Delta\theta = \Delta\phi$ bin of ~ 0.008 radian, thus reducing the number of combinatorics. Further, it is found that with proper choice of the input track co-ordinates (A track is represented by a 12-dimensional hit vector in θ, ϕ space), a principal component transformation can be carried out which leads to a parametric space with only two independent variables when the track momentum becomes large so that all the trajectories are nearly linear. This aspect has been utilised further to reject the false tracks particularly when the track density is very high. It is shown in this work that this simple road finder with a PCA or ICA cut can be used to reject low momentum tracks and select $P_T \geq 2$ GeV quite efficiently with less computational efforts. This has been demonstrated using Hijing generator with jet options [1]. In addition, since the extracted momentum is close to the true value within 20%, it can also be used as a seed finder for high P_T tracks which can be further prolonged into the TPC using Kalman filter technique or even, ITS as a stand-alone detector, can also be used to know the origin of a high P_T track which might otherwise gets lost in the TPC-TRD dead zones.

II. ITS DETECTOR AND ALIROOT SIMULATION

The Inner Tracking System (ITS) consists of 6 cylindrical layers of silicon detectors, located at radii, $r = 4, 7, 15, 24, 39$ and 44 cm. It covers the rapidity range of $|\eta| < 0.9$ for all vertices located within the length of the interaction diamond ($\pm 1\sigma$), i.e. 10.6 cm along the beam direction. The number, position and segmentation of the layers are optimized for efficient track finding and high impact parameter resolution. In particular, the outer radius is determined by the necessity to match tracks with those from the Time Projection Chamber (TPC), and the inner radius is the minimum allowed by the radius of the beam pipe (3 cm). The first layer has a more extended coverage ($|\eta| < 1.98$) to provide, together with the Forward Multiplicity Detector (FMD), a continuous coverage in rapidity for the measurement

of charged particles multiplicity. Because of high particle density, pixel detectors have been chosen for the inner most two layers, and silicon drift detectors for the following two layers. The outer two layers have double sided silicon microstrip detectors. With the exception of inner most pixel layers, all others layers will also provide energy loss information in the non-relativistic region. Thus, the ITS has a stand-alone capability as a low P_T particle spectrometer.

The simulation is carried out using AliRoot, the standard ALICE simulation and reconstruction package based on the ROOT object oriented data analysis framework [7]. We use Hijing generator for background simulation. Although, analysis is confined only to the ITS sector, we include all the ALICE detectors and passive materials in AliRoot simulation with the option of magnetic field $B = 0.5 T$ in the solenoidal region. In the present work, we use a fast simulator to get reconstructed points (recpoints) from the hits. We also neglect the vertex smearing and set vertices to $(0, 0, 0)$ for all the tracks in the AliRoot simulation. We consider only those tracks which have hits in all the six ITS layers. To minimize the dispersion, we begin with all the reconstructed points in the 4th layer with a given (θ, ϕ) and look for the corresponding points in the remaining five layers within a search window of $\theta \pm \Delta\theta$ and $\phi \pm \Delta\phi$. The (θ, ϕ) co-ordinate in the 4th layer is considered to be the seed for a good track candidate if it has entries in all the following and subsequent layers within that search window. Therefore, the efficiency (ϵ) is defined as the ratio of good tracks (as defined above) divided by the total number of seeds or the reconstructed points in the 4th layer. Since, we have considered only those tracks which have entries in all six layers, the total number of rec-points in the 4th layer also corresponds to the total number of tracks or tracklets that pass through the ITS.

FIGURES

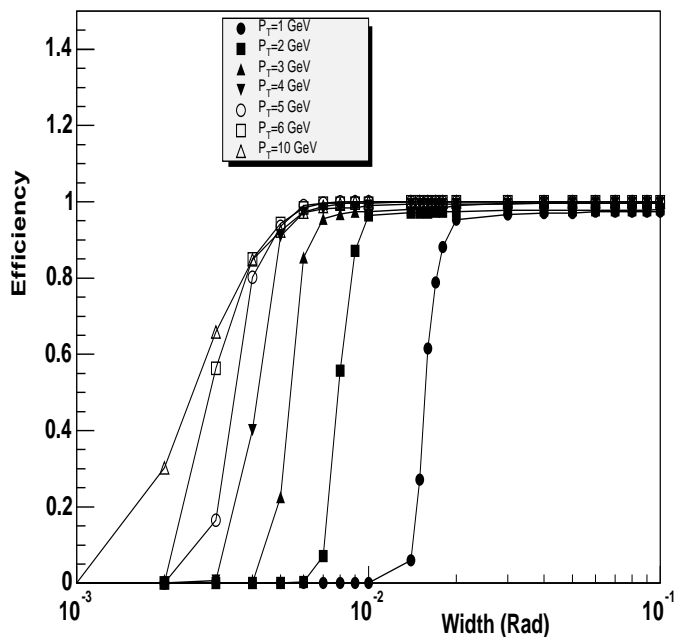


FIG. 1. The efficiency ϵ as a function of bin width ($\Delta\theta = \Delta\phi$) in radian at different P_T . For detail see the text.

Figure 1 shows the efficiency ϵ as a function of (θ, ϕ) bin width for different P_T . As can be seen from the figure, at a bin width of ~ 0.008 radian, it is possible to reject most of the low P_T tracks below 1.5 or 2.0 GeV. For this plot, we have considered only 2000 charged pions generated randomly at a fixed P_T within the full ITS acceptance. We have also taken $\Delta\phi = \Delta\theta$, although the spread in θ direction is slightly smaller than the ϕ dispersion and can be optimized further. However, the choice of $\Delta\phi = \Delta\theta$ only increases the number of combinatorics marginally and does not affect the analysis. Within this (θ, ϕ) window, we consider all the combinatorics and extract the radius of curvature (R) by a simple curvature fitting and by accepting the one for which the χ^2 is minimum. Finally, we estimated the momentum (in GeV) from the relation $P_T = .002998 B R$.

To see how well we can reconstruct the transverse momentum by only a χ^2 minimization, we generate charged pions between 0 to 10 GeV. However, this time, we chose $N = 4800$, but

restrict to only $|\eta| < 0.3$ over full azimuth so that the data volume is not too high and also the number of primaries chosen corresponds to $dN/d\eta \approx 8000$. If the fitted value of P_T is within 20% of the true P_T , we consider the estimate as true. Otherwise, it is a false estimate although the estimated χ^2 is still a minimum. Figure 2 shows the plot of number of true and false tracks as defined above as a function of P_T for three different bin widths of 0.008, 0.010 and 0.015 radians respectively. Although the original P_T distribution is uniform, the extracted momentum distribution shows non-uniformity due to poor momentum resolution. Note that for $P_T > 2$ GeV, the contribution of the false tracks remain below 10%. However, it is not possible to extract P_T below 2 GeV as the false estimate increases sharply particularly when bin width increases. It is also noticed that the contributions of the true estimates depend on the bin width to some extent. For larger bin width, the contribution of the true estimate decreases while the false estimate goes up at low momentum below $P_T < 2$ GeV. Similarly, if the bin width is too small, some of the high P_T tracks may get rejected. Therefore, it is very crucial to use proper bin width. However, as will be shown below, the dependency on the bin width can be reduced by incorporating additional techniques like principal component or independent component analysis.

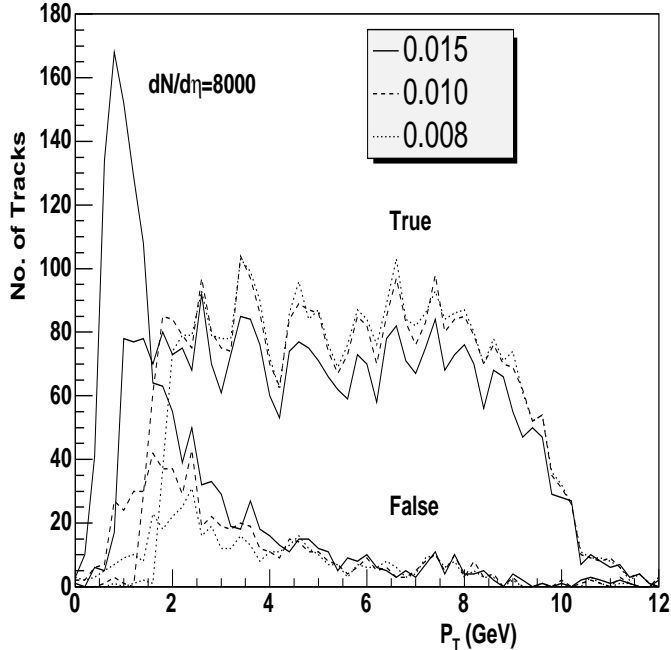


FIG. 2. The estimated true and false tracks as a function of P_T . The true tracks are having both a minimum χ^2 values as well as the extracted P_T values are within 20% of the true transverse momentum. The false tracks, although have a minimum χ^2 , do not give correct P_T estimate.

III. INDEPENDENT COMPONENT AS A HIGH PASS FILTER:

For multivariate data analysis, suitable representation is often sought as a linear transformation of the original data into a lower dimensional parametric space. Well known linear transformation methods are principal component analysis (PCA), factor analysis, and projection pursuit. Independent component analysis (ICA) is relatively a recently developed method in which the goal is to find a linear representation of non-Gaussian data so that the components are statistically independent, or as independent as possible. Such a representation seems to capture the essential structure of the data in many applications, including feature extraction and signal separation [8]. Basically, two random variables y_1 and y_2 are said to be independent if information on the value of y_1 does not give any information on the value of y_2 , and vice versa. Mathematically, if y_1 and y_2 are said to be independent if

and only if the joint probability distribution function (pdf) is factorizable so that

$$p(y_1, y_2) = p_1(y_1)p_2(y_2). \quad (1)$$

This definition extends naturally for any number of n random variables, in which case the joint pdf must be a product of n terms. Therefore, given any two functions f_1 and f_2 , the independent random variables should have the property

$$E[f_1(y_1)f_2(y_2)] = E[f_1(y_1)]E[f_2(y_2)], \quad (2)$$

where E stands for an average. A weaker form of independence is uncorrelatedness. Two random variables are said to be uncorrelated if their covariance is zero:

$$E[y_1y_2] = E[y_1]E[y_2]. \quad (3)$$

Thus, if the variables are independent, they are also uncorrelated. On the otherhand, uncorrelatedness does not imply independence for non-Gaussian random variables. There are many ICA techniques that lead to independent estimation of the parameters in the feature space. Common to all ICA analysis is the PCA transformation which is generally used as a first step to achieve uncorrelatedness. However, in the present application, we will show that by choosing the proper input parameter space, it is possible to achieve independence only through a PCA transformation although the input variables are known to be non-Gaussian.

The principal component analysis does a simple co-ordinate transformation to principal axes such that the variances of the new co-ordinates are equal to the eigen values of the covariance matrix, which is generated out of a large sample space [9,10]. We consider only the ITS layers and a single track is characterized by a M -dimensional hit vector $h = (h_1, h_2, \dots, h_M)$ whose average (H_i) and covariance (A_{ij}) are

$$H_i = \frac{1}{N} \sum_{n=1}^N (h_i)_n, \quad (4)$$

$$A_{ij} = \frac{1}{N} \sum_{n=1}^N [(h_i)_n - H_i][(h_j)_n - H_j], \quad (5)$$

where N is the number of hit vectors of the $(N \times M)$ dimensional sample space. Consider the following linear transformation:

$$X_j = \sum_{i=1}^M \omega_{ij} h_i \quad (6)$$

It can be proved [9] that the variances of \mathbf{X} are the eigenvalues λ of the dispersion matrix \mathbf{A} , when ω_{ij} represents the eigenvectors of \mathbf{A} . Hence,

$$Var(X_j) = E[X_j - E(\sum_{i=1}^M \omega_{ij} h_i)]^2 = E(\eta_j^2) = \lambda_j, \quad (7)$$

where E stands for average over N and η_j is given by

$$\eta_j = \sum_{i=1}^M \omega_{ij} (h_i - H_i). \quad (8)$$

Therefore, the PCA is tuned with a training data set in order to calculate the average and the dispersion matrices \mathbf{H} and \mathbf{A} , respectively. The experiment records a set of (θ, ϕ) pair from each layer when a charged particle enters the ITS detector. We consider all possible combinations $C = (C_1, C_2, \dots, C_M)$ and estimate the generalized distance:

$$\eta_j = \sum_{i=1}^M \omega_{ij} (C_i - H_i), \quad (9)$$

.

$$d = \frac{1}{M} \sum_{j=1}^M \eta_j^2 / \lambda_j. \quad (10)$$

It is now required that for a track candidate, d is less than some maximum value d_{max} .

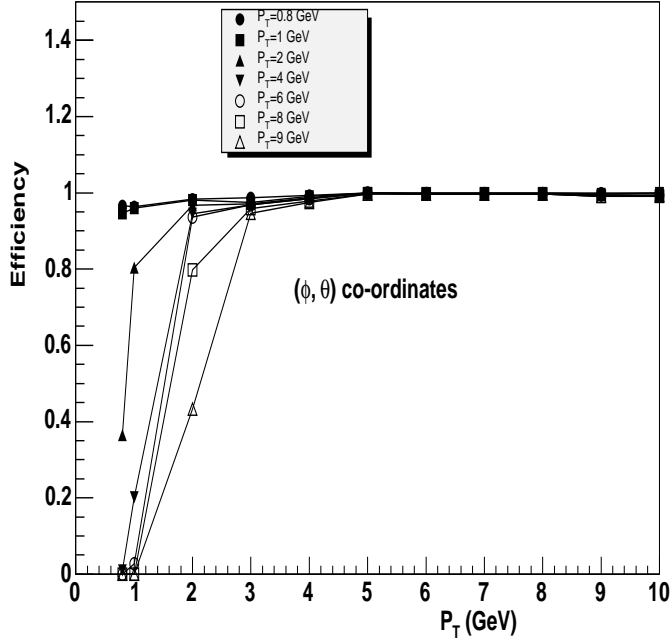


FIG. 3. The efficiency as a function of P_T . The good tracks are those for which the generalized distance d in (θ, ϕ) space is less than $d_{max} = 4.0$. The different curves correspond to training set generated at different P_T as shown in figure caption.

In the following, we carry out the PCA test with different training set. As in figure 1, we generate 2000 charged pions at different P_T . First, we consider a hit vector in (θ, ϕ) space for which $M = 12$ as a good ITS track has 6 pairs of (θ, ϕ) coordinates. Figure 3 shows the plot of efficiency of accepting good tracks after a PCA cut as a function of P_T . As in figure 1, here the efficiency is defined as the ratio of the number of track candidates for which $d \leq d_{max} = 4.0$ to the total number of good tracks N . The PCA is tuned with training data set generated at different P_T . The symbols in figure 3 show the PCA efficiency when the training set is chosen at different P_T . It is interesting to note that when the PCA is tuned with the training data set at $P_T = 0.8$ GeV, all track candidates above $P_T > 0.8$ GeV pass the PCA test (see the filled circle). However, if the PCA is tuned with a training set at higher momentum, say $P_T = 9$ GeV (see open triangles), then most of the low P_T tracks, do not pass the PCA test. This is an interesting property which can be utilised to reduce

the tracks of low P_T momentum by appropriate choice of the training data set.

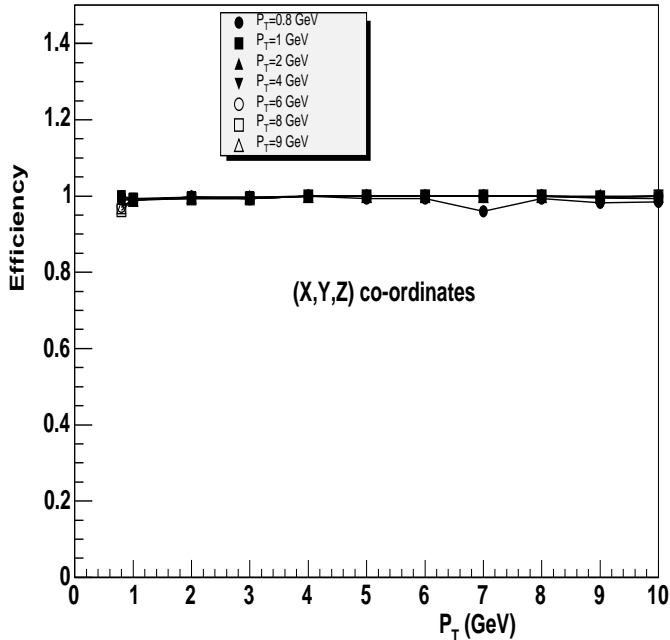


FIG. 4. The efficiency as a function of P_T . The good tracks are those for which the generalized distance d in (x, y, z) space is less than $d_{max} = 4.0$.

We have also carried out similar exercise by considering a hit vector in (x, y, z) co-ordinates. Figure 4 shows the corresponding plot as that of figure 3. However, with the choice of the cartesian co-ordinates, PCA does not have any discriminating power. This aspect can be understood if we examine the number of independent variables which can be obtained through a PCA transformation. Figure 5 shows the plot of number of independent variables (out of 12 η^2 , we consider only those variable whose values are significant and are above a given threshold) as a function of P_T . Notice that as P_T increases, the number of independent variables reduces to two which is a characteristic of all straight trajectories which can be described by only two independent variables. Such behaviour we do not find, if the input variables are chosen from the cartesian space. Therefore, PCA transformation in (θ, ϕ) space is nearly equivalent to an ICA transformation and can be used as a high pass filter for high P_T tracks.

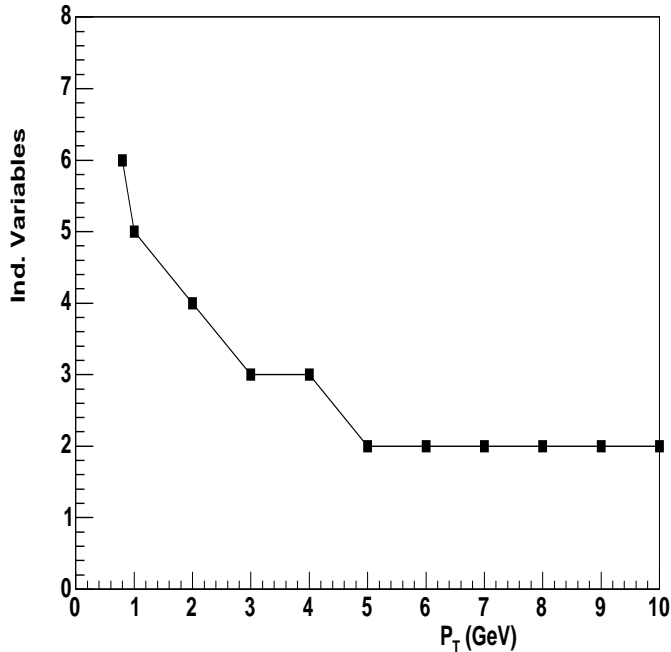


FIG. 5. The number of independent variables as a function of P_T (θ, ϕ) space.

IV. ROAD FINDER WITH PCA

In the following, we consider the road finder with the combined action of PCA and χ^2 minimization. The steps are as follows: (a) First, we consider all the reconstructed points in the 4th layer. Starting with a given (θ, ϕ) , we pick up all the points in the remaining 5 layers within a search window of $\theta \pm \Delta\theta$ and $\phi \pm \Delta\phi$. (b) Second, we consider all the combinatorics and accept those which qualify a PCA test with $d \leq 4.0$. The PCA parameters are tuned with a training set generated at $P_T = 3.0$ GeV². (c) Next, we extract the best radius parameter (R) through a minimum χ^2 curvature fitting. Therefore, at this stage, only one combination is retained for which the χ^2 is minimum. Finally, the P_T (in GeV) is extracted

²We have optimized P_T at 3.0 GeV for training so that low P_T tracks below ~ 2 GeV can be rejected.

through the relation $P_T = 0.002998 B R$ where $B = 0.5 T$. As in figure 2, figures (6 – 8) now show the contributions of true and false estimates at different track densities both with (steps a , b and c) and without PCA cut (steps a and c). With inclusion of PCA, the true estimates become independent of bin widths as can be seen prominently in figure 8 where the track density is very high. This is an attractive feature as we need not optimize too much on the bin width as long as it is close to 0.008 radian or higher. Although, slight higher in bin width increases the number of combinatorics, it still safer to allow little larger width so that we do not loose too much low P_T tracks. Another important aspect of the inclusion of PCA test is that the false P_T estimation below 2 GeV reduces drastically. In short, with a PCA cut ($d \leq 4.0$) and a bin width of ~ 0.008 radian, it is possible to extract most of the high P_T tracks above 2 GeV with good efficiency.

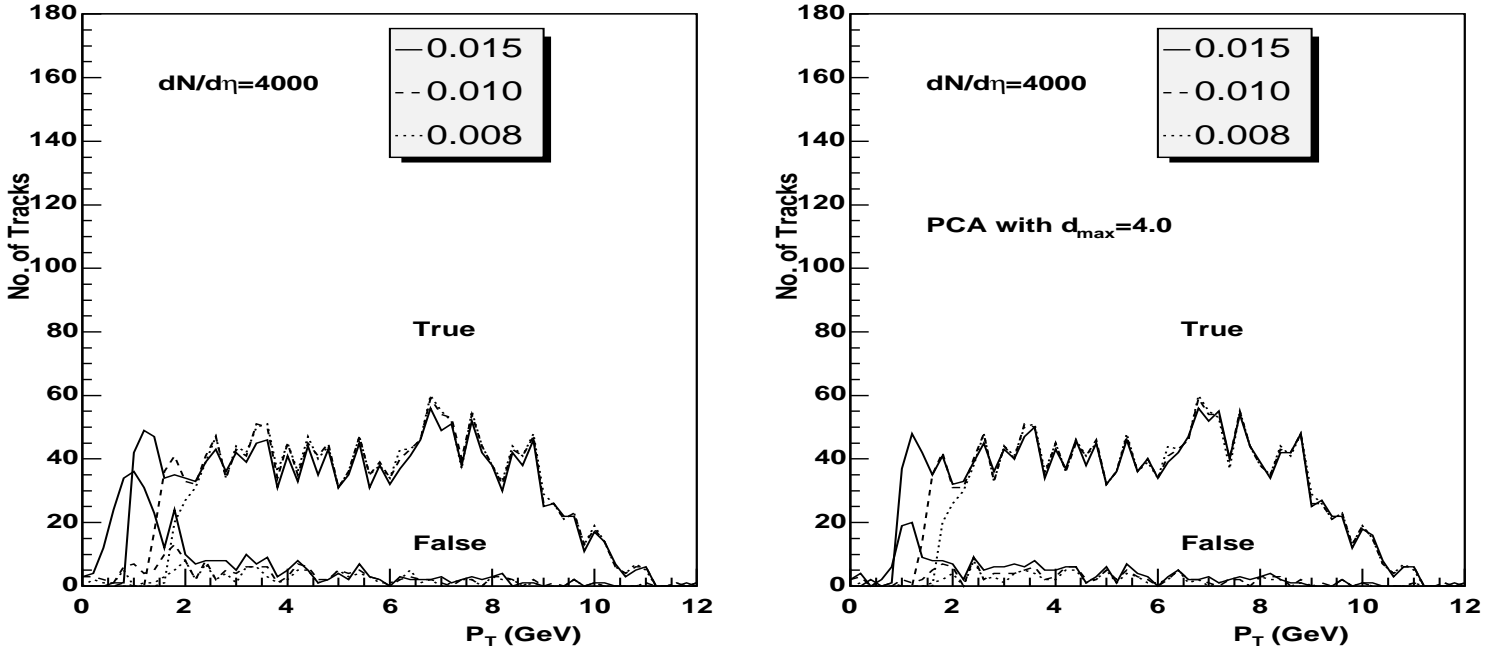


FIG. 6. The estimated true and false tracks as a function of P_T both without (left) and with (right) PCA cut.

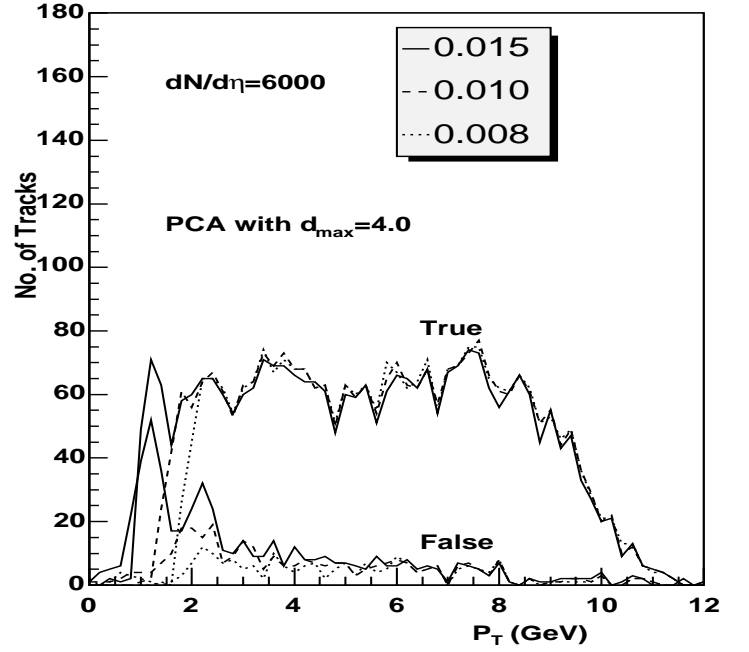
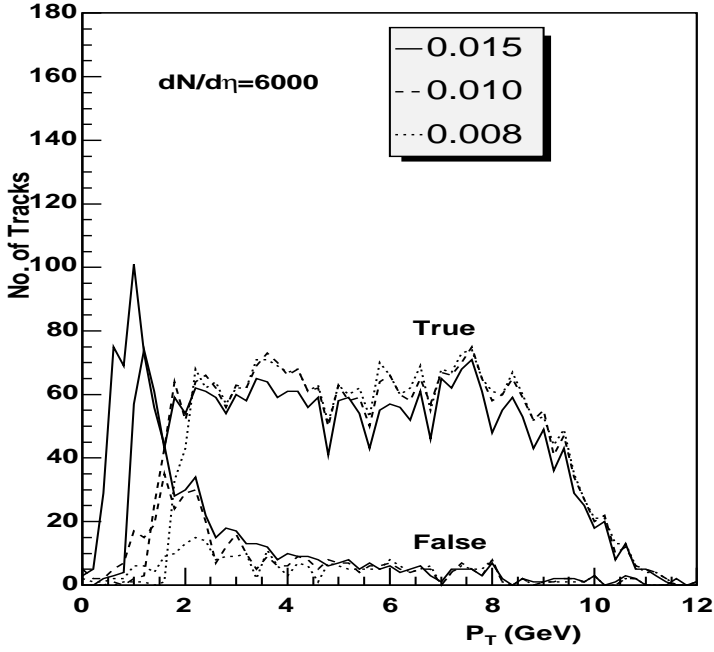


FIG. 7. The estimated true and false tracks as a function of P_T both without (left) and with (right) PCA cut.

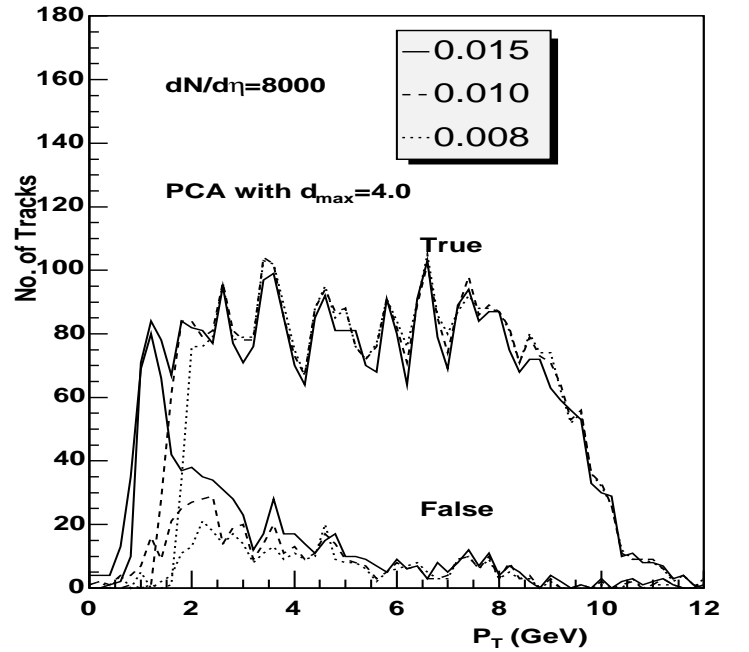
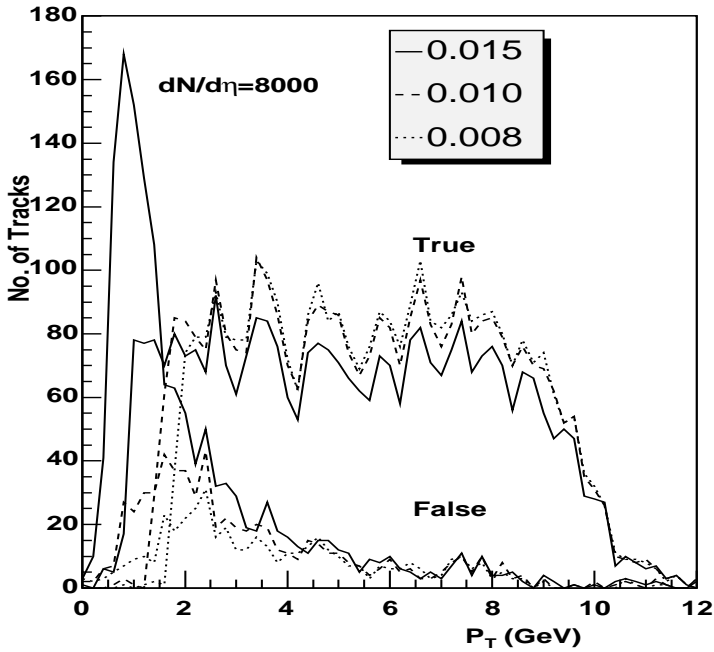


FIG. 8. The estimated true and false tracks as a function of P_T both without (left) and with (right) PCA cut.

V. HLT EFFICIENCY WITH HIJING BACKGROUND

In the following, we carry out more realistic analysis using Hijing event generator. Figure 9 shows the P_T distribution of a single Hijing event for $|\eta| < 0.3$ over full azimuth with jet options. These P_T distribution corresponds to the simulated P_T of the rec-points found only at the 4th layer. For the present purpose, we may consider it as a representation of the track density distribution inside the ITS. Figure 10 shows the P_T distribution which is obtained after the HLT cut as discussed before with a bin width of 0.008 radian and $d_{max} = 4.0$. Note that in figure 10, we have only plotted those tracks having a $P_T > 2$ GeV obtained using the HLT algorithm as discussed before. These tracks are mostly due to the jet events.

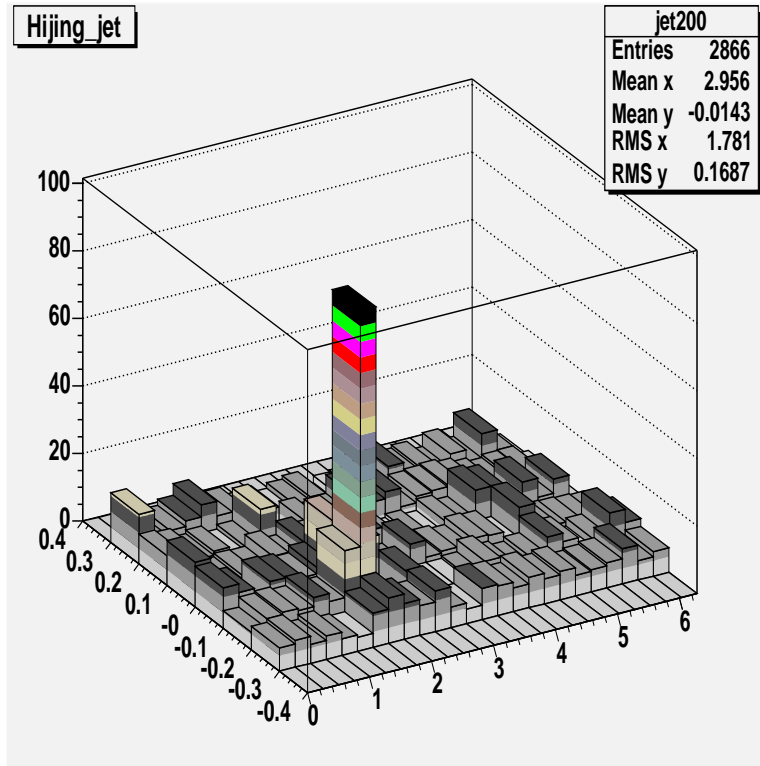


FIG. 9. The P_T distribution of recpoints of ITS 4th layer simulated using hijing event generator with jet option. Here, the bin widths are $\Delta\eta = 0.25$ and $\Delta\theta = 0.1$ respectively. This is the typical jet-cone width. Again, these widths are used only for binning in the plot. Note that this width is different from the bin width of 0.008 radian used in the HLT road finder algorithm.

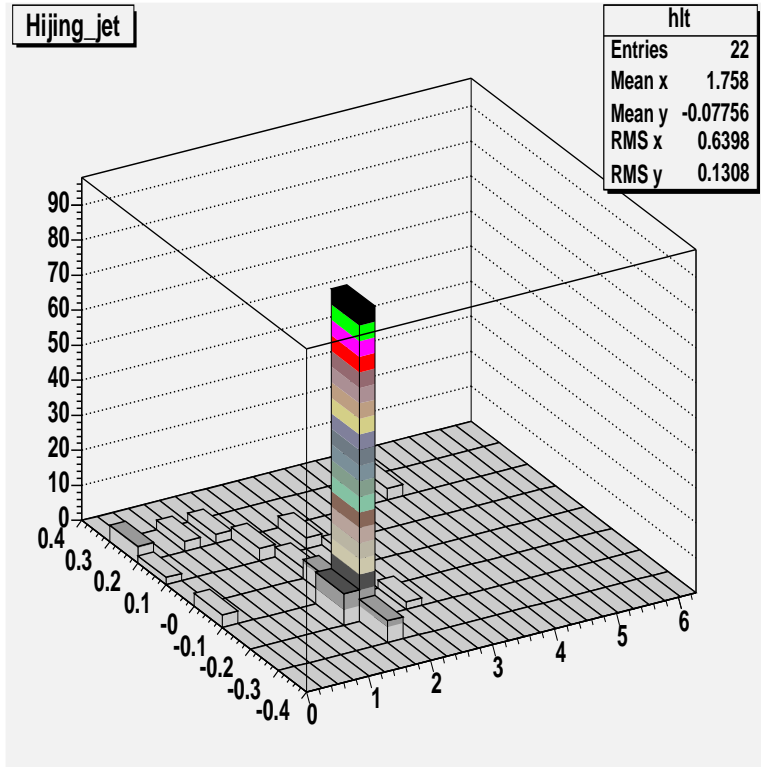


FIG. 10. Same as figure 9, but with HLT algorithm

VI. CONCLUSION

In this report, it is shown that the Inner Tracking System (ITS) of ALICE detector can be used for triggering high P_T particles as stand-alone device. The seed for the trigger road can be selected some where from the middle layer in order to have minimum dispersion both in θ and ϕ directions. It is found that most of the background low P_T tracks can be rejected by confining the search window to a narrow bin width of $\Delta\theta = \Delta\phi = 0.008$ radian. In order to estimate the transverse momentum, it is required to consider all the combinatorics inside

a given search window which may go up when the track multiplicity is high. However, it is shown that the number many false combinatorics can be reduced to an acceptable levels through a PCA test followed by a least square minimization. Using Hijing event generator, it is shown here that the ITS can be used to trigger charged particles for P_T above 2 GeV or more. The proposed HLT algorithm with ITS can be used to trigger high P_T jet particles with good efficiency.

APPENDIX: A

The ALICE detector consists of a central detector system, covering mid-rapidity ($|\eta| \leq 0.9$) over the full azimuth, and several forward systems. The central system includes, from the interaction vertex to the outside, six layers of high resolution silicon detectors (Inner Tracking System-ITS), a Time projection Chamber (TPC)-the main tracking device of the experiment, a transition radiation detector for electron identification (TRD), and a particle identification array (Time Of Flight-TOF). The central system which is installed inside a large solenoidal magnet with field of $\leq 0.5 T$ also includes an ring imaging Cherenkov detector ($|\eta| \leq 0.6$, 56.6° azimuthal coverage) for the identification of high momentum particle (High Momentum Particle Identification Detector HMPID), and an electromagnetic calorimeter ($|\eta| \leq 0.12$, 100° azimuthal coverage) consisting of arrays of high density crystals (PHOton Spectrometer-PHOS). The large rapidity systems include a muon spectrometer ($-4.0 \leq \eta \leq -2.4$), a photon counting detector (Photon Multiplicity Detector-PMD, on the opposite side), an ensemble of multiplicity detectors (FMD) in the forward rapidity region (up to $\eta = 5.1$). A system of scintillators and quartz counters (T_0 and V_0) will provide fast trigger signals, and two sets of neutron and hadron calorimeter, located at 0° and about $90 m$ away from the interaction vertex, will measure the impact parameter (Zero Degree Calorimeter-ZDC). An absorber positioned very close to the vertex shields the muon spectrometer. The muon spectrometer consists of a dipole magnet, five tracking stations, an iron wall (muon filter) to absorb remaining hadrons, and two trigger stations behind the

muon filter.

REFERENCES

- [1] *ALICE Physics Performance Report (PPR)*, Volume I- CERN/LHCC 2003-049; <http://alice.web.cern.ch/Alice>.
- [2] A. Nicolaucig, M. Mattavelli, and S. Carrato, *Compression of TPC Data in the ALICE Experiment*, ALICE-PUB-2001-51 Version 1.0, 22-10-2001, Nuclear Instruments and Method, **A487**, 542 (2002).
- [3] D. Favretto, A. K. Mohanty, F. Carminati, and K. Safarik *Optimization of frequency tables for static Huffman compression of ALIRO raw data*, ALICE-INT-2003.
- [4] A. K. Mohanty, D. Favretto, F. Carminati, and K. Safarik *Existence of Dynamical Scaling in the Temporal Signal of Time Projection Chamber*, ALICE-INT-2003-013 version 1.0, 28-03-2003, physics/0401013.
- [5] ALICE HLT collaboration, *ALICE High Level Trigger Conceptional Design Report*, January 2002; http://www.kip.uni-heidelberg.de/ti/L3/CDRFinal_CERN-tilsn.pdf.
- [6] C. Loizides et al., Submitted to IEEE-TNS, Sep 2003; physics/0310052.
- [7] <http://alisoft.cern.ch/offline>.
- [8] A. Hyvarinen, and E. Oja, Neural Network, **13**, 411-430 (2000).
- [9] M. G. Kendall, and A. Stuart, *The Advanced Theory of Statistics*, 3rd ed., Vol. 3, Ch. Griffin and Company, London, 1976, p. 294.
- [10] D. Dutta, A. K. Mohanty, R. K. Choudhury, and Phool Chand, Nuclear Instruments and Methods in Physics Research, **A404**,445-454 (1998).